ACS APPLIED MATERIALS & INTERFACES

Research Article

www.acsami.org

Self-Assembly of Electron Donor–Acceptor-Based Carbazole Derivatives: Novel Fluorescent Organic Nanoprobes for Both One- and Two-Photon Cellular Imaging

Jinfeng Zhang,[†,‡] Wencheng Chen,[†,‡] Sergii Kalytchuk,[‡] King Fai Li,[§] Rui Chen,[†,‡] Chihaya Adachi,[*,¶] Zhan Chen,[†,‡,∥] Andrey L. Rogach,[‡] Guangyu Zhu,[⊥] Peter K. N. Yu,[‡] Wenjun Zhang,[†,‡] Kok Wai Cheah,[§] Xiaohong Zhang,[*,#] and Chun-Sing Lee[*,†,‡]

[†]Center of Super-Diamond and Advanced Films (COSDAF), City University of Hong Kong, Kowloon, Hong Kong & City University of Hong Kong Shenzhen Research Institute, Shenzhen, Guangdong, P. R. China

[‡]Department of Physics and Materials Science and [⊥]Department of Biology and Chemistry, City University of Hong Kong, 83 Tat Chee Avenue, Kowloon, Hong Kong SAR 999077, P. R. China

[§]Department of Physics and Institute of Advanced Materials, Hong Kong Baptist University, Kowloon Tong, Hong Kong SAR 999077, P. R. China

[¶]Center for Organic Photonics and Electronics Research (OPERA), Kyushu University, 744 Motooka, Nishi-ku, Fukuoka 819-0395, Japan

[∥]Nano-organic Photoelectronic Laboratory, Technical Institute of Physics and Chemistry, Chinese Academy of Sciences, Beijing 100190, P. R. China

[#]Institute of Functional Nano & Soft Materials (FUNSOM), Jiangsu Key Laboratory for Carbon-Based Functional Materials & Devices, and Collaborative Innovation Center of Suzhou Nano Science and Technology, Soochow University, Suzhou, Jiangsu 215123, P. R. China

Supporting Information

ABSTRACT: In this study, we report fluorescent organic nanoprobes with intense blue, green, and orange-red emissions prepared by self-assembling three carbazole derivatives into nanorods/nanoparticles. The three compounds consist of two or four electron-donating carbazole groups linked to a central dicyanobenzene electron acceptor. Steric hindrance from the carbazole groups leads to noncoplanar 3D molecular structures favorable to fluorescence in the solid state, while the donor–acceptor structures endow the molecules with good two-photon excited emission properties. The fluorescent organic nanoprobes exhibit good water dispersibility, low cytotoxicity, superior resistance against photodegradation and photobleaching. Both one- and two-photon fluorescent imaging were shown in the A549 cell line. Two-photon fluorescence imaging with the fluorescent probes was demonstrated to be more effective in visualizing and distinguishing cellular details compared to conventional one-photon fluorescence imaging.

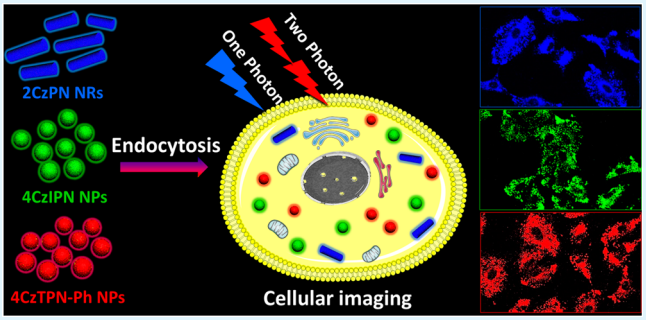

KEYWORDS: *self-assembly, electron donor–acceptor, carbazole derivatives, fluorescent organic nanoprobes, two-photon cellular imaging*

1. INTRODUCTION

The development of fluorescence probes for biomedical applications in diagnostic, imaging, and sensing has attracted considerable attention.[1−3] Fluorescent imaging has many advantages including simple operating procedures, easily maneuverable instruments, and wide availability of low-cost imaging reagents.[4] Moreover, fluorescence imaging can also provide high sensitivity and high spatiotemporal resolution images with more dynamic details at subcellular levels.[5−8] In the last couple of decades, fluorescent nanoparticles (NPs) have drawn much research interest because of their better biocompatibility and remarkable optical properties including broader absorption spectra, size-tunable emissions, larger Stokes shifts and better photostability compared with conventional organic dyes.[9−13] In particular, inorganic semiconductor quantum dots (Qdots)[14−17] and fluorescent polymer dots

Received: March 17, 2016
Accepted: April 21, 2016
Published: April 21, 2016

DOI: 10.1021/acsami.6b03259
ACS Appl. Mater. Interfaces 2016, 8, 11355−11365

Scheme 1. Schematic Illustration of the Preparation of Blue/Green/Red FONs by a Reprecipitation Method for One- and Two-Photon Cellular Imaging

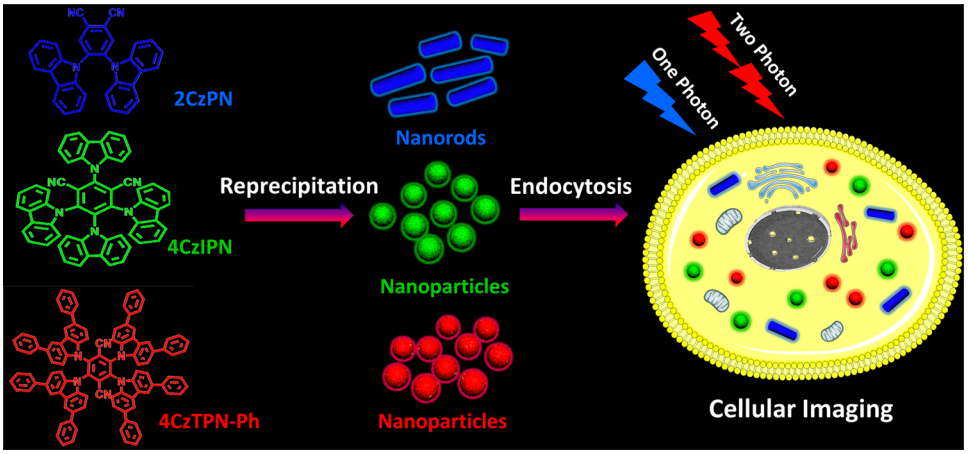

(Pdots)[18−21] represent two of the most popular classes of nanoprobes because of their high brightness. However, before wide clinical applications, further research is needed to address issues such as potential toxicity[22−24] and biodegradability.[25] In the past few years, fluorescent organic nanoprobes (FONs) based on small molecules have emerged as promising competitors in terms of their wide chemical tailorability, structural variability, low toxicity, and good biodegradability.[26−36] However, a major challenge for the development of high-performance FONs is that the fluorescent intensity of many organic molecules would be greatly decreased or completely quenched upon self-assembly into nanostructures because of intermolecular $\pi-\pi$-stacking interaction.[37] For example, pyrene is a small organic molecule with strong blue fluorescence in dilute solution. However, solid pyrene tends to form excimers through $\pi-\pi$ stacking, exhibiting dramatically reduced photoluminescence quantum yield (PLQY) and large emission red shift accompanied by broad full-width at half-maximum.[38] On the other hand, many reported FONs using short-wavelength excitations (e.g., UV) can cause cellular damage and undesirable background signals as a result of autofluorescence.[26−29,31] Furthermore, the use of short-wavelength excitation also limits the application of these FONs in animal models because of poor penetration depth.[39]

Previous studies on the structure−property correlation of nonlinear-optical materials demonstrated that an electron donor−acceptor-based molecular architecture is conducive to the process of two-photon absorption (TPA) because of the electron push−pull effect that reinforces intramolecular charge transfer (ICT) upon excitation.[40,41] However, ICT-based organic fluorophores are typically featured with spatially separated frontier molecular orbitals, which often lead to lower PLQYs because of the forbidden electronic transition.[42] Therefore, the development of donor−acceptor-based organic emitters with simultaneous high fluorescence and effective TPA is still a challenge.

During the past decades, carbazole derivatives have received considerable attention for their applications in organic optoelectronic devices including organic light-emitting devices, organic photovoltaic devices, transistors, etc.[43−50] Owing to its rigid and planar aromatic stucture,[51] carbazole has been used as a skeleton to make high-performance emitting materials.[52−54] In particular, several donor−acceptor compounds obtained by linking different acceptor groups to carbazole as the donor have been shown to have impressive TPA coefficients.[55−58] This enables such carbazole-based emitters to be excited with near-infrared sources, thus avoiding the problems of photodamaging, autofluorescence, and shallow penetration depth associated with short-wavelength excitation.[59−64] Unfortunately, most reported carbazole-based organic molecules show poor water solubility, which hinders their wider biomedical application.

In this work, we attempt to develop high-performance FONs with simultaneous high solid-state fluorescence, two-photon excited emission, and good water dispersibility by addressing the mentioned issues with three carbazole derivatives. The three compounds are obtained by joining two or four carbazole electron-donating groups to a central dicyanobenzene electron acceptor (Scheme 1).[43] In addition to the highly fluorescent carbazole moieties, the two electron-accepting cyano groups are beneficial to achieving high PLQYs because of their function of suppressing nonradiative deactivation.[65] Attachment of the bulky and rigid carbazole groups around the central benzene ring would cause steric hindrance, leading to noncoplanar and 3D molecular structures.[43] With these 3D structures, $\pi-\pi$ stacking between molecules would be reduced and enable the materials to have good fluorescence in the solid state. FONs were prepared by the self-assembly of three carbazole derivatives into NPs/nanorods (NRs) of 80−200 nm size (Scheme 1). The large surface area-to-volume ratios of these nanostructures endow these FONs with good water dispersibilities; even the original molecules have poor water solubilities. The three FONs not only show typical one-photon fluorescent emission of respectively red, green, and blue but also display high-contrast two-photon fluorescent imaging in A549 cells. Together with their good biocompatibilities and superior photostabilities, FONs based on fluorescent carbazole derivatives are considered to be promising high-performance probes for bioimaging.

2. EXPERIMENTAL SECTION

2.1. Materials. 4,5-Bis(carbazol-9-yl)-1,2-dicyanobenzene (2CzPN) and 2,4,5,6-tetrakis(carbazol-9-yl)-1,3-dicyanobenzene (4CzIPN) were obtained from Xi'an Polymer Light Technology Corp., while 2,3,5,6-tetrakis(3,6-diphenylcarbazol-9-yl)-1,4-dicyanobenzene (4CzTPN-Ph) was synthesized in house as reported previously.[43] 3-(4,5-Dimethylthiazol-2-yl)-2,5-diphenyltetrazolium bromide (MTT) was obtained from Sigma-Aldrich and used after drying in vacuo for 24 h. Dulbecco's modified Eagle's medium (DMEM), fetal bovine serum (FBS), Dulbecco's phosphate-buffered

DOI: 10.1021/acsami.6b03259
ACS Appl. Mater. Interfaces 2016, 8, 11355−11365

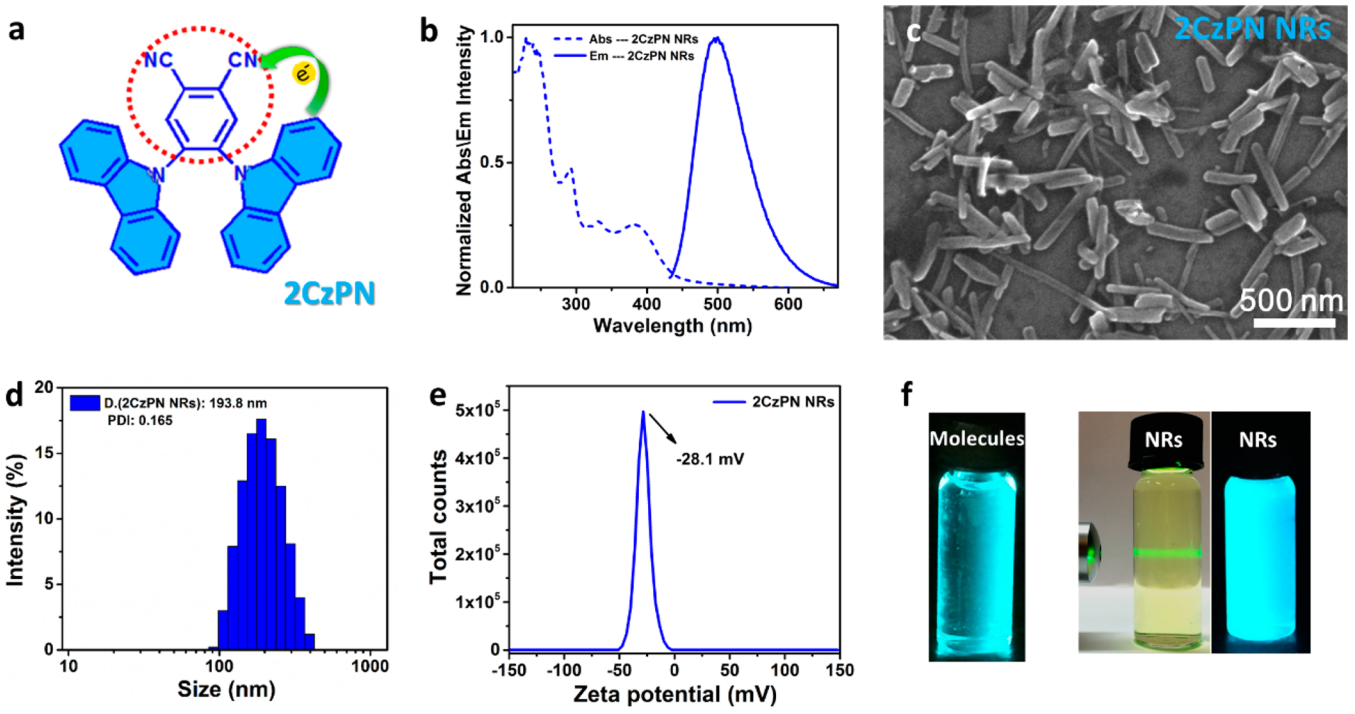

Figure 1. (a) Electron donor−acceptor-based molecular structure of 2CzPN. (b) Normalized absorbance and fluorescence spectra of 2CzPN NRs dispersed in deionized water (excitation wavelength, 380 nm; path length, 1 cm). (c) SEM image of 2CzPN NRs. (d) DLS and PDI measurements. (e) ζ potential of the 2CzPN NRs. (f) Photographs of 2CzPN molecules dissolved in THF under UV light (left) and 2CzPN NRs dispersed in deionized water under room light (middle) and UV light (right) (concentration: 40 μg/mL).

saline (PBS), trypsin/ethylenediaminetetraacetic acid (EDTA; 0.5% trypsin and 5.3 mM EDTA tetrasodium), and the antibiotic agents penicillin and streptomycin (100 U/mL) were purchased from Life Technologies. Deionized water with a resistivity higher than 18.4 MΩ·cm was collected from an in-line Millipore RiOs/Origin water purification system. Unless otherwise noted, all chemicals were obtained from commercial suppliers and used as received.

2.2. FON Preparation. FONs were prepared using the well-documented reprecipitation method. In a typical procedure, a 1 mg/mL solution of 2CzPN, 4CzIPN, and 4CzTPN-Ph dissolved in tetrahydrofuran (THF) was prepared. A total of 200 μL of the as-prepared THF solution was quickly dropped into 5 mL of deionized water under vigorous stirring at room temperature for 10 min. Dispersions of the FONs were obtained by further sonication for another 15 min under room temperature to ensure complete THF evaporation.

2.3. FON Characterization. The sizes and morphologies of the FONs were investigated using scanning electron microscopy (SEM; Philips XL-30 FEG). The SEM samples were prepared by drying a dispersion of the FONs on a silicon substrate, followed by coating of a 2 nm gold layer. Dynamic light scattering (DLS) measurements and ζ potentials were carried out using a Malvern Zetasizer instrument employing a 4 mW helium−neon laser (λ = 632.8 nm) and equipped with a thermostatic sample chamber.

2.4. Optical Properties and Photostability Measurements. UV−visible spectra were recorded using a Cary 50Conc UV−visible spectrophotometer. Fluorescence spectra were recorded on a Cary Eclipse fluorescence spectrophotometer. The PLQYs of the FONs were measured with a fluorescence spectrometer (FLS920P, Edinburgh Instruments) equipped with a 120 mm integrating sphere with a BENFLEC coated inner face (Edinburgh Instruments). The fluorescence lifetime data were obtained using a Edinburgh Analytical Instruments F900. Time-dependent photodegradation and photobleaching experiments were carried out using a xenon lamp (150 W) equipped with a filter passing light from 400 to 700 nm (100 mW/cm^2).

2.5. TPA Cross-Sectional Measurements. The TPA cross section σ was measured by a TPA-induced fluorescence method. The value of the TPA cross section σ was obtained by comparing their TPA-induced up-converted fluorescence to that of Rhodamine 6G in methanol at a concentration of about 2×10^{-5} mol/L.

$$\sigma_{new} = \sigma_{ref}\left(\frac{\eta 1_{ref} C_{ref} \eta_{ref}}{\eta 1_{new} C_{new} \eta_{new}}\right)\left(\frac{\langle F\rangle_{new}}{\langle F\rangle_{ref}}\right)$$

where η is the fluorescence quantum yield, C is the concentration, n is the refractive index, and $\langle F\rangle$ is the integrated area of the up-converted fluorescence signal. The new and ref subscripts refer to the sample and standard reference solutions, respectively. For the femtosecond pulse experiment, the excitation source was from an optical parametric amplifier (TOPAS-C) pumped by a mode-locked Ti:sapphire laser oscillator/amplifier system (Spectra Physics). The output wavelength in this study was from 800 to 950 nm. The pulse width of the laser was about 120 fs, and its repetition rate was 1 kHz. The fluorescence was perpendicularly collected into an Acton monochromator system by a telescope system. The monochromator connected with a sensitive GaAs photomultiplier tube (Hamamatsu) was used as the recorder for the TPA-induced up-converted fluorescence. The power of the femtosecond laser was real-time measured and used to correct the fluorescence signal. The fluctuation of the laser power was less than 3%.

2.6. One-Photon/Two-Photon Cellular Imaging. A549 cells were cultured with DMEM (with 10% FBS and 1% penicillin/streptomycin) in 5% CO_2 at 37 °C in a humidified incubator. The cells were trypsinized and resuspended on 60 mm culture plates, and 2 mL of the medium was combined with 1.0 mL of a cell suspension. The cells were then seeded on 6-well plates, which were then placed in an incubator at 37 °C overnight with 5% CO_2 for 24 h. The FON dispersions were respectively added to each plate and carefully mixed (final concentration: 8 μg/mL). The treated cells were returned to the incubator (37 °C, 5% CO_2) for 4 h. After incubation, the plates were washed thoroughly with sterile PBS. Finally, one-photon fluorescent images of the cells were recorded with a Nikon ECLIPSE 80i

DOI: 10.1021/acsami.6b03259
ACS Appl. Mater. Interfaces 2016, 8, 11355−11365

fluorescent microscope. Two-photon fluorescent images of the cells were performed using a Leica TCS SP5 laser scanning confocal microscope with 800 nm two-photon excitation (TPE).

2.7. Cytotoxicity by MTT Assay. The A549 cells were seeded on 96-well plates in DMEM (with 10% FBS and 1% penicillin/streptomycin) and grown overnight. After removal of the original medium in each well, 200 μL of DMEM containing predetermined concentrations of FONs was added to the designated wells. The final concentration of these FONs on each plate ranged from 6.25 to 100 μM. After 24 h of incubation at 37 °C, the original medium in each well was removed. Subsequently, 180 μL of DMEM (without FBS) and 20 μL of a MTT stock solution (5 mg/mL in PBS) were added and incubated for another 4 h. Then the medium containing MTT was completely removed, followed by the addition of 200 μL of dimethyl sulfoxide (Acros) to each well. The cell viabilities were determined by reading the absorbance of the plates at 540 nm using a BioTek Powerwave XS microplate reader. The cells incubated with a serum-supplemented medium represent 100% cell survival. Five replicate wells were run for each concentration.

3. RESULTS AND DISCUSSION

Our proposed strategy for preparing highly emissive FONs for one- and two-photon cellular imaging is illustrated in Scheme 1. The chemical structures of the three carbazole derivatives (2CzPN, 4CzIPN, and 4CzTPN-Ph) are shown in Scheme 1. Upon reprecipitation, 2CzPN self-assembled into blue-emitting NRs, while 4CzIPN and 4CzTPN-Ph gave respectively green- and red-emitting NPs. The nanostructured FONs can be successfully taken up by cancer cells via endocytosis showing strong one-photon fluorescence as well as high-contrast two-photon fluorescence.

Figure 1a shows the electron donor−acceptor-based molecular structure of 2CzPN, where electrons can be transferred from the peripheral carbazolyl groups to the central dicyanobenzene unit, indicating ICT characteristics. The photophysical properties of free 2CzPN molecules in THF and NRs are displayed in Figures 1b and S1 and Table 1.

Table 1. Summary of the Photophysical Properties of 2CzPN, 4CzIPN, and 4CzTPN-Ph Molecules Dissolved in THF and 2CzPN, 4CzIPN, and 4CzTPN-Ph NRs/NPs in Deionized Water[a]

sample	λ_{abs} (nm)[b]	λ_{em} (nm)/λ_{ex} (nm)	PLQY (%)/λ_{ex} (nm)	τ (ns)[c]
2CzPN molecules	369	503/400	21.5/371	16.3
2CzPN NRs	382	503/400	19.4/385	3.7 (τ_1), 12.9 (τ_2)
4CzIPN molecules	370	518/400	33.5/371	18.6
4CzIPN NPs	379	518/400	11.9/385	5.5 (τ_1), 19.9 (τ_2)
4CzTPN-Ph molecules	501	578/500	6.6/355	3.7
4CzTPN-Ph NPs	515	588/500	3.6/350	6.5

[a] λ_{abs} = peak of absorption; λ_{em} = peak of emission; λ_{ex} = excitation wavelength. [b] The reddest absorption maximum. [c] τ represents the fluorescent lifetime of the measured samples.

Absorption and emission spectra of 2CzPN dissolved in THF and 2CzPN NRs dispersed in deionized water, respectively, were measured. Here, the 2CzPN molecules dissolved in THF exhibit an absorption peak at 369 nm (Table 1). In comparison, the 2CzPN NRs exhibit a red-shifted absorption spectrum possibly due to aggregate effects in the nanostructures. On the other hand, the 2CzPN molecules and 2CzPN NRs show no observable shift in their emission peak at 503 nm, indicating that π−π stacking is effectively suppressed. The PLQYs of the free 2CzPN molecules dissolved in THF and the 2CzPN NRs dispersed in water were determined to be 21.5% and 19.4%, respectively. The high PLQY makes 2CzPN NRs an excellent nanoprobe for cellular fluorescence imaging. Figure 1c displays an SEM image of the 2CzPN NRs showing a well-defined and regular rod shape with average length and width of 308 and 52 nm, respectively. DLS measurement (Figure 1d) presents a hydrodynamic diameter of 193.8 nm and a polydispersity index (PDI) value of 0.165. The 2CzPN NRs have a negative ζ potential of −28.1 mV due to the formation of a hydrogen bond by the attraction of slightly positive hydrogen atoms in water to the lone pair on the nitrogen atom in a nitrile,[66] which will stabilize the NRs in an aqueous medium by electrostatic repulsion (Figure 1e). Figure 1f displays photographs of the 2CzPN molecules dissolved in a THF solution under UV light (left) and the 2CzPN NRs dispersed in deionized water under room light (middle) and UV irradiation (right). Both free 2CzPN molecules and 2CzPN NRs emit intense blue fluorescence. The presence of NRs was also confirmed by shining a green laser beam through the 2CzPN dispersion to clearly show the Tyndall effect.

Figure 2a shows an electron donor−acceptor-based molecular structure of 4CzIPN, where electrons can be transferred from the peripheral carbazolyl groups toward the central dicyanobenzene unit. Figures 2b and S1 and Table 1 display the photophysical properties of free 4CzIPN molecules dissolved in a THF solution and 4CzIPN NPs dispersed in deionized water. Here, the absorption peak of free 4CzIPN molecules dissolved in THF is at 370 nm. The absorption peak of the NPs also exhibits a red shift with respect to the dissolved molecules, while the NPs show emission maxima at the same peak wavelength of 518 nm. The PLQYs of the dissolved molecules and NPs were determined to be 33.5 and 11.9%, respectively. Figure 2c shows an SEM image of the 4CzIPN NPs in the form of well-defined nanospheres of ∼100 nm diameter. DLS measurement (Figure 2d) presents a hydrodynamic diameter of 94.27 nm and a PDI value of 0.197. The 4CzIPN NPs also show a negative ζ potential around −24.9 mV (Figure 2e). Figure 2f displays photographs of the 4CzIPN molecules dissolved in a THF solution under UV light (left) and the 4CzIPN NPs dispersed in water under room light (middle) and UV irradiation (right). Both free 4CzIPN molecules and 4CzIPN NPs show strong green fluorescence. The Tyndall effect can be clearly observed, confirming the presence of 4CzIPN NPs in water.

An electron donor−acceptor-based molecular structure of 4CzTPN-Ph is shown in Figure 3a. 4CzTPN-Ph exhibits orange-red fluorescence in both molecular and nanometer forms. The photophysical properties of free 4CzTPN-Ph molecules dissolved in a THF solution and 4CzTPN-Ph NPs dispersed in deionized water are shown in Figures 3b and S1 and Table 1. We found that the absorbance spectrum of the 4CzTPN-Ph molecule in THF shows an absorption peak at about 500 nm (Figure S1), but this peak disappears in the absorbance spectrum of 4CzTPN-Ph NPs in water (Figure 3b). In fact, the structureless, board absorption peak at around 500 nm in 4CzTPN in THF can be attributed to ICT absorption. The absorption of a sample depends on many factors such as the dielectric constant of the solvent, solvent−solute/solute−solute interaction, etc. It has been demonstrated that the

DOI: 10.1021/acsami.6b03259
ACS Appl. Mater. Interfaces 2016, 8, 11355−11365

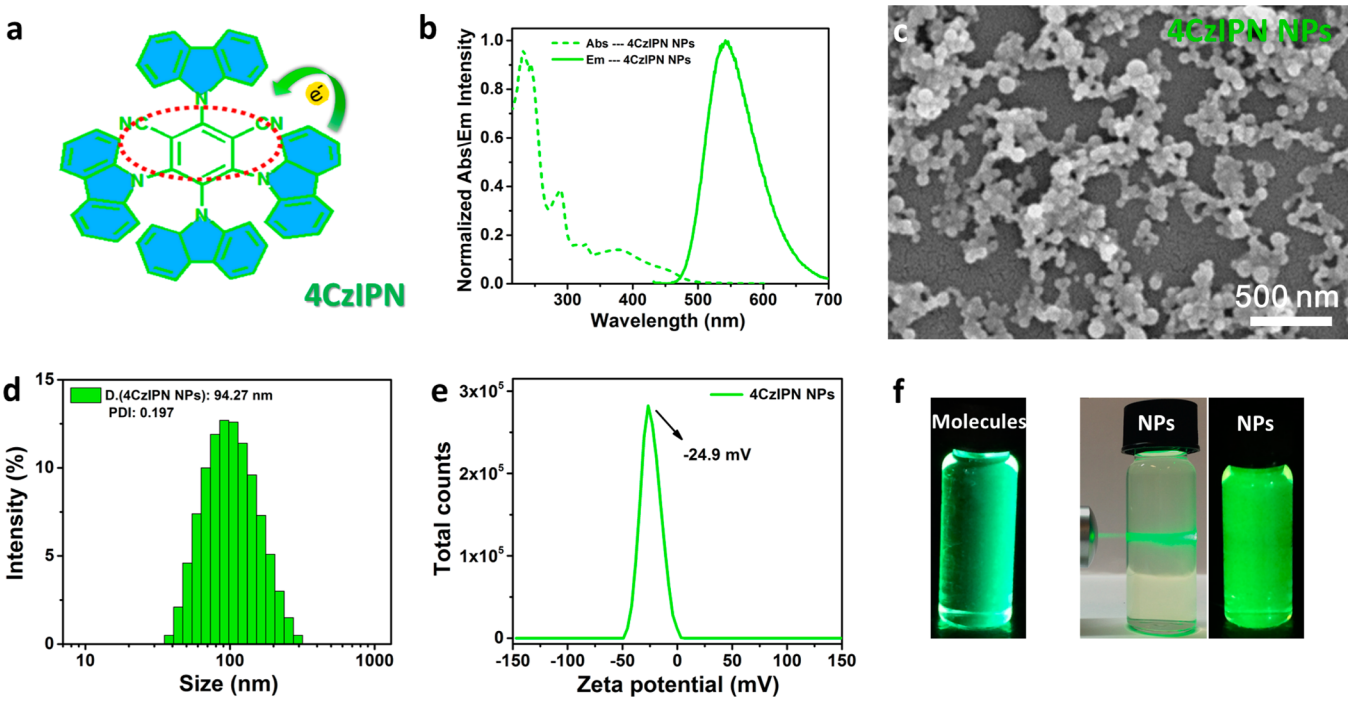

Figure 2. (a) Electron donor−acceptor-based molecular structure of 4CzIPN. (b) Normalized absorbance and fluorescence spectra of 4CzIPN NPs dispersed in deionized water (excitation wavelength, 380 nm; path length, 1 cm). (c) SEM image of 4CzIPN NPs. (d) DLS and PDI measurements and (e) ζ potential of the 4CzIPN NPs. (f) Photographs of 4CzIPN molecules dissolved in THF under UV light (left) and 4CzIPN NPs dispersed in deionized water under room light (middle) and UV light (right) (concentration: 40 μg/mL).

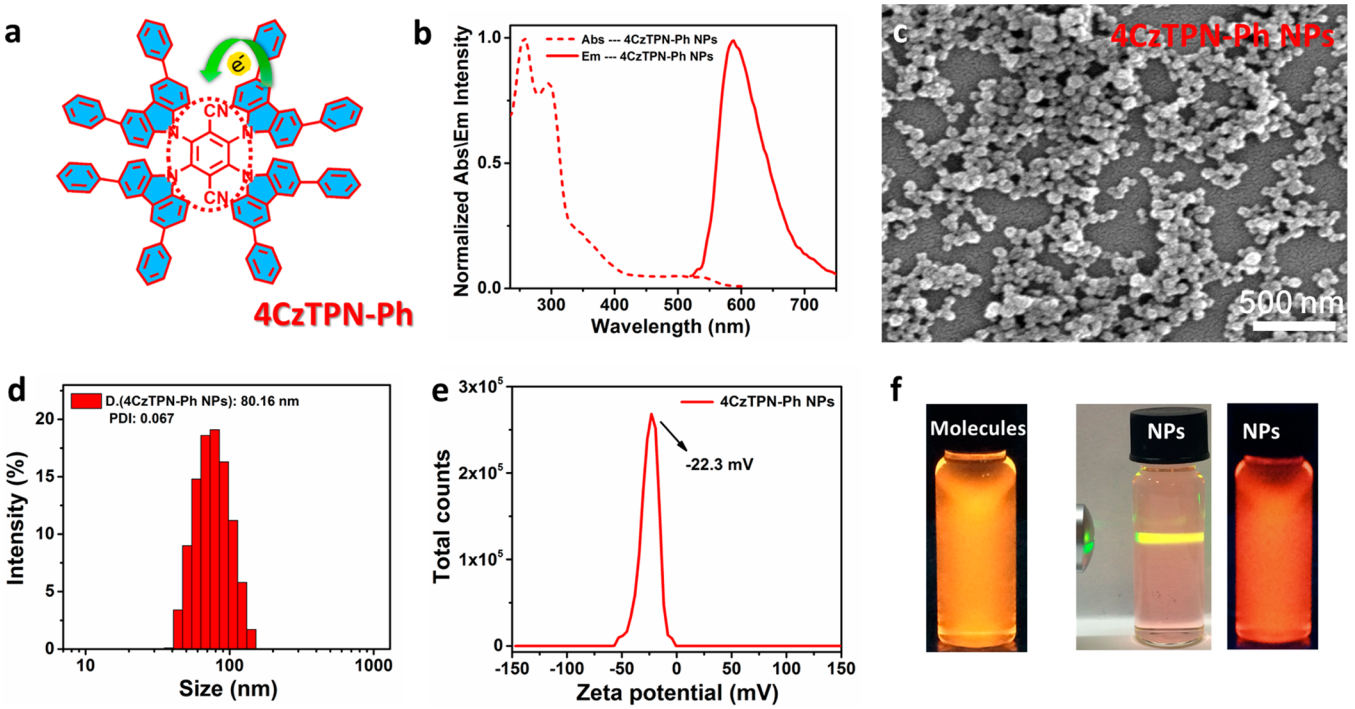

Figure 3. (a) Electron donor−acceptor-based molecular structure of 4CzTPN-Ph. (b) Normalized absorbance and fluorescence spectra of 4CzTPN-Ph NPs dispersed in deionized water (excitation wavelength, 500 nm; path length, 1 cm). (c) SEM image of 4CzTPN-Ph NPs. (d) DLS and PDI measurements and (e) ζ potential of the 4CzTPN-Ph NPs. (f) Photographs of 4CzTPN-Ph molecules dissolved in THF under UV light (left) and 4CzTPN-Ph NPs dispersed in deionized water under room light (middle) and UV light (right) (concentration: 40 μg/mL).

protonated form of the sample can eliminate the charge-transfer band completely.[67] As mentioned above, a cyano group with electron-deficient properties can physically interact with slightly positive hydrogen atoms in water, which may cause the absorption peak at about 500 nm in the 4CzTPN NPs to disappear. The PLQYs of 4CzTPN-Ph dissolved in THF and NPs dispersed in water are determined to be 6.6% and 3.6%, respectively. Compared with the PLQYs of the blue and green

DOI: 10.1021/acsami.6b03259
ACS Appl. Mater. Interfaces 2016, 8, 11355−11365

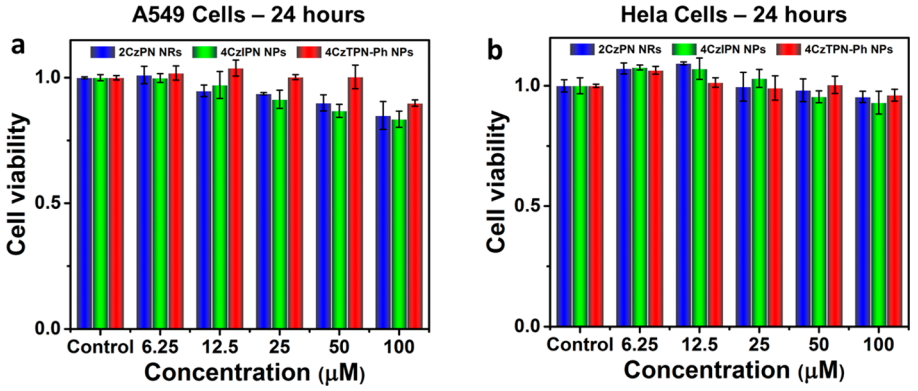

Figure 4. Cell viabilities of different FONs against (a) the A549 cell line and (b) the Hela cell line at various concentrations after 24 h of incubation, indicating that the as-prepared FONs have low cytotoxicity and good biocompatibility. Data represent the mean value ± standard deviation and n = 5.

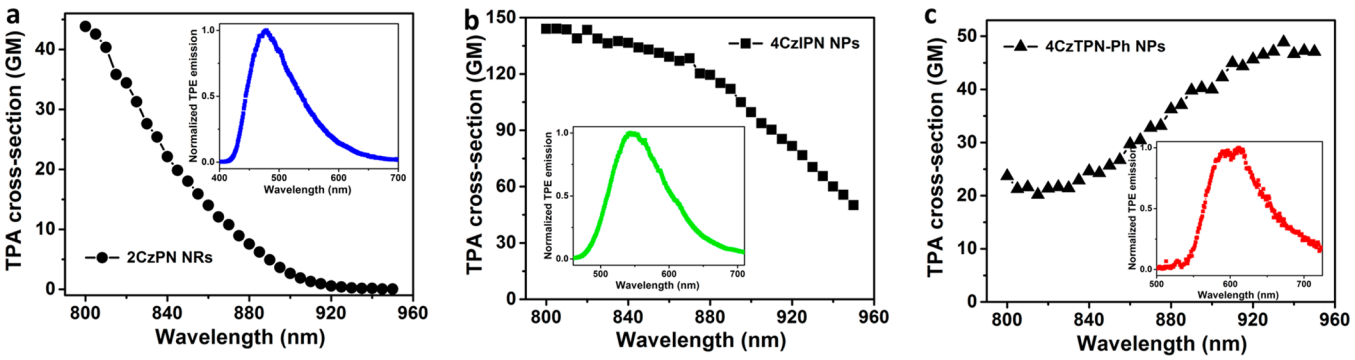

Figure 5. TPA cross sections of (a) 2CzPN NRs, (b) 4CzIPN NPs, and (c) 4CzTPN-Ph NPs dispersed in deionized water. Insets are the corresponding normalized emission spectra under TPE at 800 nm.

counterparts discussed above, those of organic red-emitting 4CzTPN-Ph are relatively lower because of the limitation of the energy-gap law.[68] However, the emission is strong enough for both one- and two-photon cellular imaging. Figure 3c shows an SEM image of the 4CzTPN-Ph NPs, indicating that the as-prepared 4CzTPN-Ph NPs possess a monodispersed spherical shape with diameter below 100 nm. To confirm that the morphologies of the FON samples were not affected by the sample preparation process, we also observed morphologies of the FON samples prepared by freeze-drying their dispersions. As shown in Figure S2, the morphologies of FONs are basically the same as those prepared by drying directly on a silicon wafer (Figures 1c, 2c, and 3c). DLS measurement (Figure 3d) presents a hydrodynamic diameter of 80.16 nm and a PDI value of 0.067. Similar to the other two carbazole derivatives, the formation of a hydrogen bond in a nitrile group leads to a negative ζ potential of −22.3 mV on the surface of the 4CzTPN-Ph NPs (Figure 3e). These negative charge-induced Columbic repulsions keep them from self-aggregation in the dispersions. Figure 3f displays photographs of the 4CzTPN-Ph molecules dissolved in a THF solution under UV light (left) and the 4CzTPN-Ph NPs dispersed in water under UV irradiation (right). Both free 4CzTPN-Ph molecules and 4CzTPN-Ph NPs show strong orange-red emission. The presence of 4CzTPN-Ph NPs in water was also confirmed by clear observation of the Tyndall effect (middle of Figure 3f). It is worth noting that our as-prepared carbazole-based nanoprobes show better water dispersibility compared with the previously reported free carbazole derivatives. That is because nanomaterials can achieve a high surface-to-volume ratio by reducing their particle sizes. The significantly increased surface area can increase the dissolution rate and saturation solubility of the as-prepared nanostructures, which eventually leads to good water dispersibility. Table 1 and Figures S3−S8 also show the fluorescence lifetimes and fluorescence decay curves of 2CzPN, 4CzIPN, and 4CzTPN-Ph molecules dissolved in THF and 2CzPN, 4CzIPN, and 4CzTPN-Ph NRs/NPs dispersed in deionized water. The orders of magnitude of the fluorescence lifetime in molecules and NRs/NPs are similar, suggesting that the formation of excimers is effectively suppressed.

Interestingly, we found that the three compounds have similar structures but self-assembled into different nanostructures. We tentatively attributed this phenomena to the different characteristics of the individual molecular structures. In blue-emitter 2CzPN, there are less carbazole groups attached in the central benzene compared with the other two molecules. The two cyano groups are exposed outward and ready to contact with other molecules easily in solid. Because of the donor−acceptor structure ($\delta^+-\delta^-$), carbazoles display positive charges (δ^+) and cyano groups negative charges (δ^-) in dipole resonance. This feature may lead to donor−acceptor dipole−dipole supramolecular interaction, which can help to form 1D nanostructures.[69] The form of supramolecular interaction can follow the form of $\delta^+-\delta^-\cdots\delta^+-\delta^-\cdots\delta^+-\delta^-\cdots\delta^+-\delta^-$.... In contrast, more carbazole/phenylcarbazole groups in 4CzIPN and 4CzTPN-Ph cause large steric hindrance, which reduces the exposure of cyano groups to their surroundings, leading to reduced donor−acceptor dipole−dipole supramolecular interaction. This may be the reason why 4CzIPN and 4CzTPN-Ph

DOI: 10.1021/acsami.6b03259
ACS Appl. Mater. Interfaces 2016, 8, 11355−11365

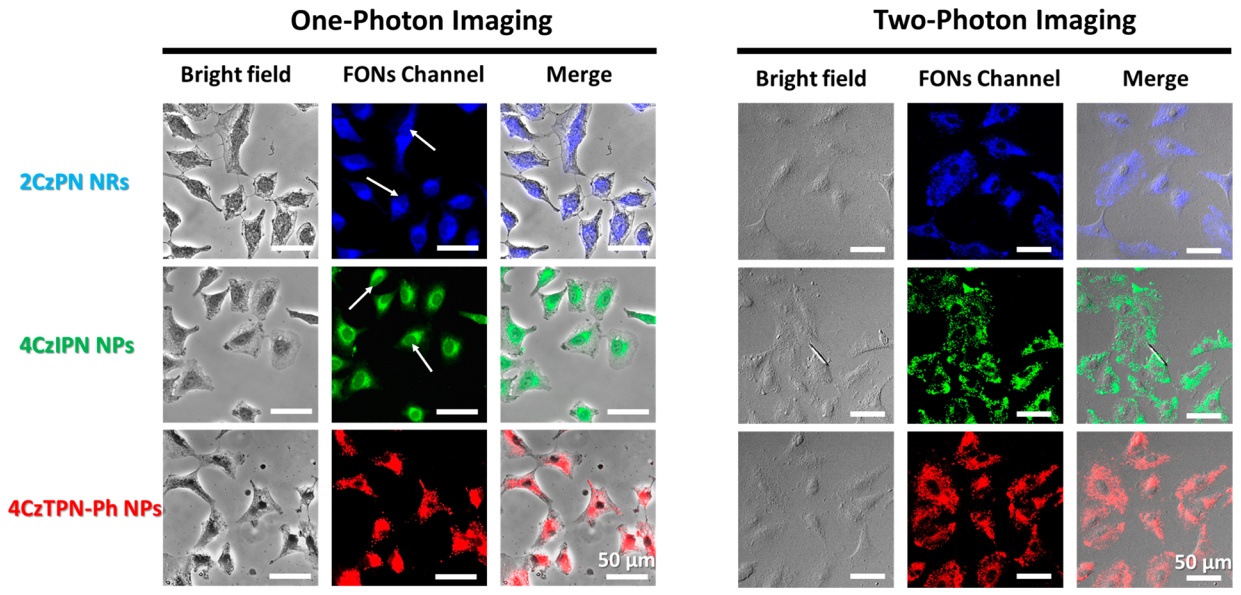

Figure 6. One-photon/two-photon cellular imaging and localization of the three FONs, monitored respectively with a fluorescence microscope (excitation wavelength: 380−420 nm) and a laser scanning confocal fluorescence microscope (excitation wavelength: 800 nm) in a A549 cell (final concentration: 8 μg/mL): (left column) bright-field channel; (middle column) FON channel; (right column) overlap of the above images. The scale bar is 50 μm.

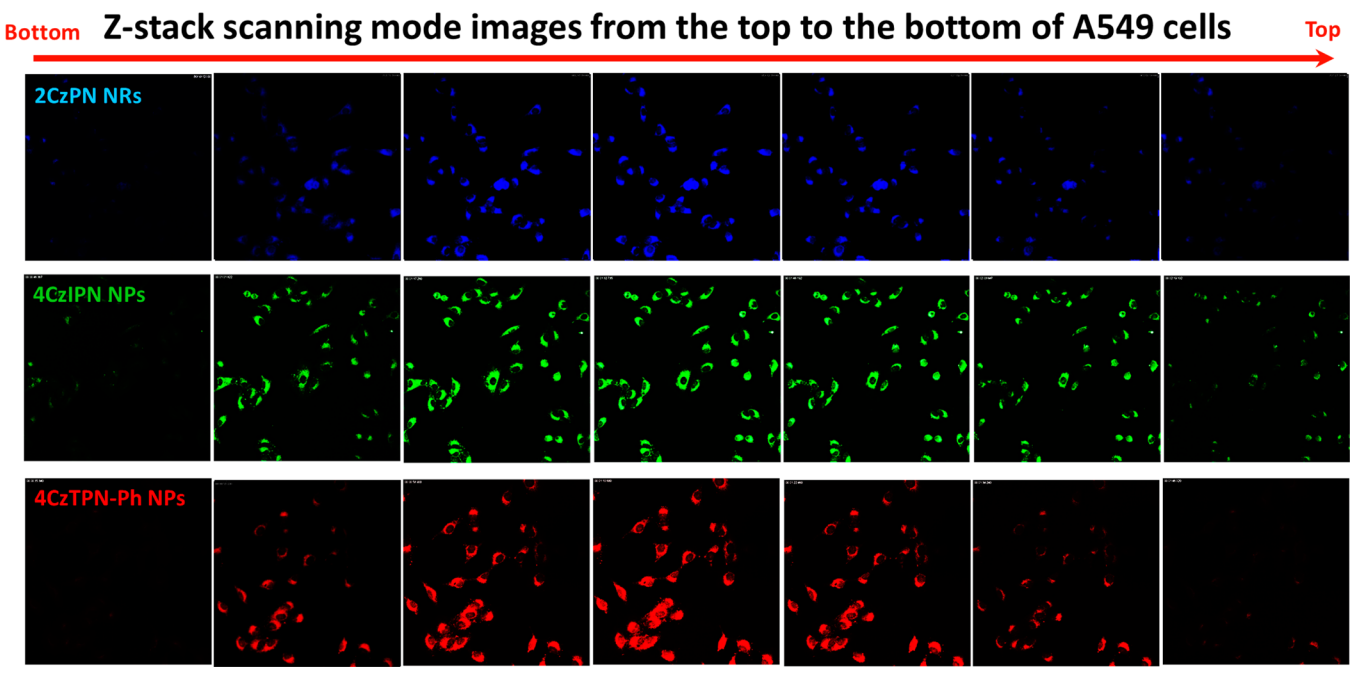

Figure 7. Confocal laser scanning microscopy z-stack images of the A549 cell incubated with the 2CzPN, 4CzIPN, and 4CzTPN-Ph nanoprobes, respectively, indicating that the FONs can be successfully taken up into the cells (z step size, 1.08 μm; z volume, 6.5 μm).

form NPs instead of NRs. The largest negative ζ potential of 2CzPN also supports this view.

The cytotoxicities of the blue/green/red FONs after 24 h of incubation with the A549 human lung cancer cells and Hela human cervical cancer cells were evaluated using MTT assay (Figure 4). The cell viabilities of these two cell lines are over ~90% after incubation for 24 h. When the incubation period extends to 48 h (Figure S9), the cell viabilities for both cell lines are ~85% even at a concentration of 100 μM. The results demonstrate that the as-prepared nanomaterials have low cytotoxicity toward both cancer cell lines at different concentrations, confirming that the as-prepared FONs have good biocompatibility.

To confirm the two-photon properties of our as-prepared FONs, we measured both TPA cross sections and TPE emission spectra of the FONs under excitation at 800 nm using femtosecond laser pulses. As displayed in Figure 5, 2CzPN NRs, 4CzIPN NPs, and 4CzTPN-Ph NPs display TPA cross-sectional values of 45, 144, and 24 GM (Goeppert−Mayer unit, with 1 GM = 10^{-50} cm^4·s/photon) at 800 nm, respectively, determined by using Rhodamine 6G in methanol as the reference (the TPA cross-sectional value of Rhodamine 6G at

DOI: 10.1021/acsami.6b03259
ACS Appl. Mater. Interfaces 2016, 8, 11355−11365

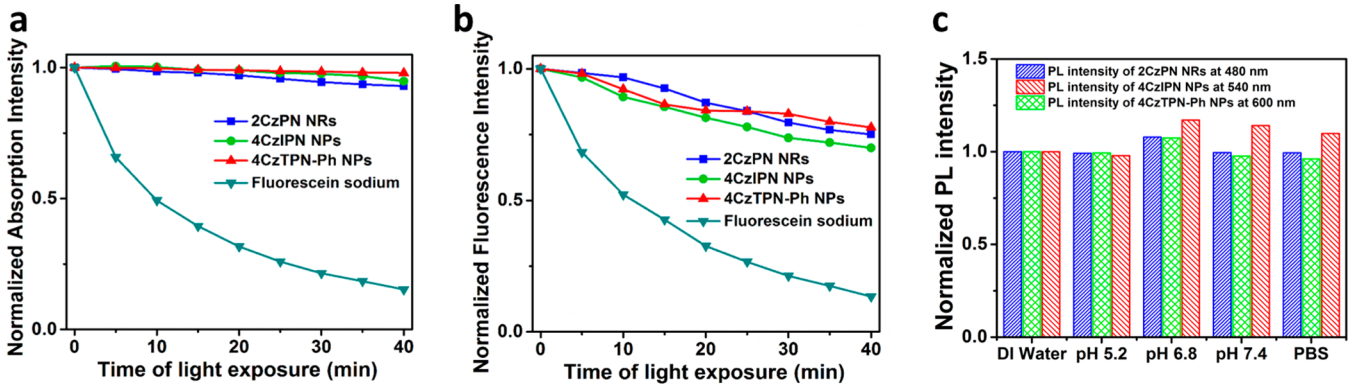

Figure 8. Photostability of the as-prepared FONs. (a) Time-dependent photodegradation and (b) photobleaching of the FONs compared with fluorescein sodium. (c) Fluorescence intensity of the FONs at different emission wavelengths in PBS (pH 7.4) and other buffer solutions with different pH values (5.2, 6.8, and 7.4) compared with that in deionized water.

800 nm is 65 GM). Furthermore, the two-photon capabilities of the different FONs were also proven by TPE emission spectra under 800 nm femtosecond laser irradiation, as shown in the insets of Figure 5. These emission wavelengths are similar to those of the original FONs under one-photon excitation, as displayed above. These results confirm the FONs' potential for TPA imaging.

To investigate the imaging capability of the three FONs, both one- and two-photon fluorescence images were obtained respectively with fluorescence microscopy and laser scanning confocal fluorescence microscopy in a A549 cell. For the one-photon imaging experiments, samples were excited at 380−420 nm. The TPE fluorescence imaging experiments were performed under excitation at 800 nm. As shown in Figure 6, intense cytoplasmic blue, green, and red fluorescence signals from the 2CzPN, 4CzIPN, and 4CzTPN-Ph nanoprobes, respectively, were clearly observed. After the bright-field and fluorescence channels overlapped, the FONs were found to mainly accumulate around the nuclear region. A *z*-stack of confocal laser scanning microscopy images, as shown in Figure 7, confirms that the FONs can be successfully taken up and localized in the cytoplasm and perinuclear region within the cells rather than just being adsorbed on the surfaces of the cells.

Furthermore, it is worth noting that, in one-photon fluorescence imaging, a homogeneous fluorescence signal can be observed in the entire cytoplasm without further details; fluorescence in the nucleus can also be observed, as indicated by the white arrows shown in Figure 6. For comparison, two-photon fluorescence imaging for FONs shows more cytoplasmic details with no fluorescence signal from the nuclear region. This shows that while the FONs have been internalized into the cytoplasm, they cannot go into the cell nucleus. The fluorescence signal from the nucleus for the one-photon fluorescence images is likely to be due to autofluorescence of the nucleus.[70] To further prove this point, control groups without incubation with the FONs in both one- and two-photon imaging experiments were carried out. As we explained above, weak autofluorescence stemming from the nucleus is observed in both blue and green channels in one-photon fluorescence images when excited at 380−420 nm, as displayed in Figure S10, while no autofluorescence could be found in two-photon fluorescence images. In addition, there is no signal observed in the red channel of one-photon fluorescence images because autofluorescence of the nucleus cannot reach the red emission range. These improvements demonstrate that two-photon fluorescence imaging is more effective in differentiating and distinguishing of cellular details than the one-photon fluorescence imaging of FONs. All of the results proved that carbazole-based FONs are promising nanoprobes for both one- and two-photon fluorescence imaging.

To further confirm the potential of FONs to serve as effective fluorescence imaging agents, their photostabilities were compared with that of fluorescein sodium. Fluorescein sodium is one of the most stable commercially available fluorescent organic dyes widely used for bioimaging.[34,36] In addition, it also has an excitation wavelength similar to those of the present FONs. Fluorescein sodium is thus used as a reference for comparing the photostability under the same conditions. As depicted in Figure 8, there is little degradation in absorbance and less bleaching in fluorescence of the three FONs compared with fluorescein sodium after 40 min of irradiation with a xenon lamp. For instance, the absorbance of the 4CzTPN-Ph NPs retained more than 97.9% of the original value, while the absorbance of fluorescein sodium was degraded to 15.2% within the same irradiation time (Figure 8a). On the other hand, the fluorescence intensity of the 4CzTPN-Ph NPs decreased to 77.7% after continuous irradiation for 40 min, while the fluorescein sodium was greatly bleached to 13.4% (Figure 8b). We also investigated the chemostability of the as-prepared FONs in different environments such as PBS (pH 7.4) and different pH value (5.2, 6.8, and 7.4) solutions obtained by mixing buffer solutions of citric acid and Na_2HPO_4 in different ratios. We used these three pH values because the micro-environment in a tumor usually has a pH of ∼6.85 and endo/lysosomes in cancer cells experience even lower pH values of 5.0−5.5. As displayed in Figure 8c, no fluorescence quenching was observed at their maximum emission peaks (2CzPN NRs at 480 nm, 4CzIPN NPs at 540 nm, and 4CzTPN-Ph NPs at 600 nm) in both PBS and other buffer solutions with different pH values compared with that in deionized water, demonstrating that all three FONs exhibit good photostability. Besides the photostabilities, we also confirmed the monodispersity stabilities of these NRs and NPs. As shown in Figure S11, no obvious agglomeration and aggregation can be observed in both photographs of the FONs dispersed in deionized water and the corresponding SEM images after 2 weeks of storage, indicating their good size stabilities. These results reveal that the carbazole-based FONs exhibit superior photostabilities and

DOI: 10.1021/acsami.6b03259
ACS Appl. Mater. Interfaces 2016, 8, 11355−11365

good monodispersity stabilities, which are beneficial for their potential bioimaging applications.

4. CONCLUSION

In summary, high-performance FONs of different colors were developed by using three carbazole derivatives with donor−acceptor structures, which endow them with high fluorescence upon both one- and two-photon excitation. NRs/NPs of the three carbazole derivatives obtained by reprecipitation show good biocompatibility, photostability, and water dispersibility. Cell imaging in the A549 cell line was performed with both one- and two-photon excitation with good results. The advantages of two-photon imaging showing more cellular details and less influence from the background autofluorescent signal were demonstrated. These results suggest that self-assembled nanostructures of carbazole derivatives with donor−acceptor molecular structure are promising high-performance fluorescence probes for bioimaging.

■ ASSOCIATED CONTENT

Supporting Information

The Supporting Information is available free of charge on the ACS Publications website at DOI: 10.1021/acsami.6b03259.

Absorbance and fluorescence spectra (Figure S1), SEM images (Figure S2), fluorescence decay curves (Figures S3−S8), cell viabilities of different FONs (Figure S9), control images in both one- and two-photon imaging experiments (Figure S10), and photographs and their corresponding SEM images (Figure S11) (PDF)

■ AUTHOR INFORMATION

Corresponding Authors

*E-mail: adachi@cstf.kyushu-u.ac.jp.
*E-mail: xiaohong_zhang@suda.edu.cn.
*E-mail: apcslee@cityu.edu.hk.

Notes

The authors declare no competing financial interest.

■ ACKNOWLEDGMENTS

This research was supported by the National Natural Science Foundation of China (Grant 51473138), the JST, ERATO, Adachi Molecular Exciton Engineering Project, and the Priority Academic Program Development of Jiangsu Higher Education Institutions.

■ REFERENCES

(1) Giepmans, B. N. G.; Adams, S. R.; Ellisman, M. H.; Tsien, R. Y. The Fluorescent Toolbox for Assessing Protein Location and Function. *Science* **2006**, *312*, 217−224.

(2) Chan, J.; Dodani, S. C.; Chang, C. J. Reaction-Based Small-Molecule Fluorescent Probes for Chemoselective Bioimaging. *Nat. Chem.* **2012**, *4*, 973−984.

(3) Wang, Y.; Zhou, K.; Huang, G.; Hensley, C.; Huang, X.; Ma, X.; Zhao, T.; Sumer, B. D.; DeBerardinis, R. J.; Gao, J. A Nanoparticle-Based Strategy for the Imaging of A Broad Range of Tumours by Nonlinear Amplification of Microenvironment Signals. *Nat. Mater.* **2013**, *13*, 204−212.

(4) Geng, J.; Li, K.; Ding, D.; Zhang, X.; Qin, W.; Liu, J.; Tang, B. Z.; Liu, B. Lipid-PEG-Folate Encapsulated Nanoparticles with Aggregation Induced Emission Characteristics: Cellular Uptake Mechanism and Two-Photon Fluorescence Imaging. *Small* **2012**, *8*, 3655−3663.

(5) Xuan, W.; Sheng, C.; Cao, Y.; He, W.; Wang, W. Fluorescent Probes for the Detection of Hydrogen Sulfide in Biological Systems. *Angew. Chem., Int. Ed.* **2012**, *51*, 2282−2284.

(6) Yao, J.; Yang, M.; Duan, Y. Chemistry, Biology, and Medicine of Fluorescent Nanomaterials and Related Systems: New Insights into Biosensing, Bioimaging, Genomics, Diagnostics, and Therapy. *Chem. Rev.* **2014**, *114*, 6130−6178.

(7) Hu, Q.; Gao, M.; Feng, G.; Liu, B. Mitochondria-Targeted Cancer Therapy Using a Light-Up Probe with Aggregation-Induced-Emission Characteristics. *Angew. Chem., Int. Ed.* **2014**, *53*, 14225−14229.

(8) Ghale, G.; Nau, W. M. Dynamically Analyte-Responsive Macrocyclic Host-Fluorophore Systems. *Acc. Chem. Res.* **2014**, *47*, 2150−2159.

(9) Chan, W. C.; Nie, S. Quantum Dot Bioconjugates for Ultrasensitive Nonisotopic Detection. *Science* **1998**, *281*, 2016−2018.

(10) Feng, L.; Zhu, C.; Yuan, H.; Liu, L.; Lv, F.; Wang, S. Conjugated Polymer Nanoparticles: Preparation, Properties, Functionalization and Biological Applications. *Chem. Soc. Rev.* **2013**, *42*, 6620−6633.

(11) Ding, D.; Li, K.; Liu, B.; Tang, B. Z. Bioprobes Based on AIE Fluorogens. *Acc. Chem. Res.* **2013**, *46*, 2441−2453.

(12) McVey, B. F. P.; Tilley, R. D. Solution Synthesis, Optical Properties, and Bioimaging Applications of Silicon Nanocrystals. *Acc. Chem. Res.* **2014**, *47*, 3045−3051.

(13) Xu, S.; Li, D.; Wu, P. One-Pot, Facile, and Versatile Synthesis of Monolayer Mos2/WS2 Quantum Dots As Bioimaging Probes and Efficient Electrocatalysts for Hydrogen Evolution Reaction. *Adv. Funct. Mater.* **2015**, *25*, 1127−1136.

(14) Gao, J.; Chen, K.; Luong, R.; Bouley, D. M.; Mao, H.; Qiao, T.; Gambhir, S. S.; Cheng, Z. A Novel Clinically Translatable Fluorescent Nanoparticle for Targeted Molecular Imaging of Tumors in Living Subjects. *Nano Lett.* **2012**, *12*, 281−286.

(15) Jin, Y.; Ye, F.; Zeigler, M.; Wu, C.; Chiu, D. T. Near-Infrared Fluorescent Dye-Doped Semiconducting Polymer Dots. *ACS Nano* **2011**, *5*, 1468−1475.

(16) Ye, F.; Wu, C.; Jin, Y.; Wang, M.; Chan, Y. H.; Yu, J.; Sun, W.; Hayden, S.; Chiu, D. T. A Compact and Highly Fluorescent Orange-Emitting Polymer Dot for Specific Subcellular Imaging. *Chem. Commun.* **2012**, *48*, 1778−1780.

(17) Yu, J.; Wu, C.; Tian, Z.; McNeill, J. Tracking of Single Charge Carriers in A Conjugated Polymer Nanoparticle. *Nano Lett.* **2012**, *12*, 1300−1306.

(18) Wu, C.; Chiu, D. T. Highly Fluorescent Semiconducting Polymer Dots for Biology and Medicine. *Angew. Chem., Int. Ed.* **2013**, *52*, 3086−3109.

(19) Yang, G.; Liu, L.; Yang, Q.; Lv, F.; Wang, S. A Multifunctional Cationic Pentathiophene: Synthesis, Organelle-Selective Imaging, and Anticancer Activity. *Adv. Funct. Mater.* **2012**, *22*, 736−743.

(20) Feng, L.; Zhu, C.; Yuan, H.; Liu, L.; Lv, F.; Wang, S. Conjugated Polymer Nanoparticles: Preparation, Properties, Functionalization and Biological Applications. *Chem. Soc. Rev.* **2013**, *42*, 6620−6633.

(21) Wu, K.; Zhang, J.; Fan, S.; Li, J.; Zhang, C.; Qiao, K.; Qian, L.; Han, J.; Tang, J.; Wang, S. Plasmon-Enhanced Fluorescence of PbS Quantum Dots for Remote Near-Infrared Imaging. *Chem. Commun.* **2015**, *51*, 141−144.

(22) Yong, K. T.; Law, W. C.; Hu, R.; Ye, L.; Liu, L.; Swihart, M. T.; Prasad, P. N. Nanotoxicity Assessment of Quantum Dots: From Cellular to Primate Studies. *Chem. Soc. Rev.* **2013**, *42*, 1236−1250.

(23) Tsoi, K. M.; Dai, Q.; Alman, B. A.; Chan, W. C. W. Are Quantum Dots Toxic? Exploring the Discrepancy Between Cell Culture and Animal Studies. *Acc. Chem. Res.* **2013**, *46*, 662−671.

(24) Smith, W. E.; Brownell, J.; White, C. C.; Afsharinejad, Z.; Tsai, J.; Hu, X.; Polyak, S. J.; Gao, X.; Kavanagh, T. J.; Eaton, D. L. In Vitro Toxicity Assessment of Amphiphilic Polymer-Coated CdSe/ZnS Quantum Dots in Two Human Liver Cell Models. *ACS Nano* **2012**, *6*, 9475−9484.

(25) Li, M.; Feng, L.; Lu, H.; Wang, S.; Chen, C. Tetrahydro[5]-helicene-Based Nanoparticles for Structure-Dependent Cell Fluorescent Imaging. *Adv. Funct. Mater.* **2014**, *24*, 4405−4412.

DOI: 10.1021/acsami.6b03259
ACS Appl. Mater. Interfaces 2016, 8, 11355−11365

(26) An, F. F.; Ye, J.; Zhang, J.; Yang, Y.; Zheng, C.; Zhang, X.; Liu, Z.; Lee, C. S.; Zhang, X. Non-Blinking, Highly Luminescent, pH- and Heavy-Metal-Ion-Stable Organic Nanodots for Bio-Imaging. *J. Mater. Chem. B* **2013**, *1*, 3144−3151.
(27) Zhang, J.; Li, S.; An, F. F.; Liu, J.; Jin, S.; Zhang, J. C.; Wang, P. C.; Zhang, X.; Lee, C. S.; Liang, X. J. Self-Carried Curcumin Nanoparticles for *In Vitro* and *In Vivo* Cancer Therapy with Real-Time Monitoring of Drug Release. *Nanoscale* **2015**, *7*, 13503−13510.
(28) Petkau, K.; Kaeser, A.; Fischer, I.; Brunsveld, L.; Schenning, A. P. H. J. Pre- and Postfunctionalized Self-Assembled π-Conjugated Fluorescent Organic Nanoparticles for Dual Targeting. *J. Am. Chem. Soc.* **2011**, *133*, 17063−17071.
(29) Jana, A.; Devi, K. S. P.; Maiti, T. K.; Singh, N. D. P. Perylene-3-Ylmethanol: Fluorescent Organic Nanoparticles as A Single-Component Photoresponsive Nanocarrier with Real-Time Monitoring of Anticancer Drug Release. *J. Am. Chem. Soc.* **2012**, *134*, 7656−7659.
(30) Jana, A.; Nguyen, K. T.; Li, X.; Zhu, P.; Tan, N. S.; Agren, H.; Zhao, Y. Perylene-Derived Single-Component Organic Nanoparticles with Tunable Emission: Efficient Anticancer Drug Carriers with Real-Time Monitoring of Drug Release. *ACS Nano* **2014**, *8*, 5939−5952.
(31) Zhang, J.; An, F.; Li, Y.; Zheng, C.; Yang, Y.; Zhang, X.; Zhang, X. Simultaneous Enhanced Diagnosis and Photodynamic Therapy of Photosensitizer-Doped Perylene Nanoparticles via Doping, Fluorescence Resonance Energy Transfer, and Antenna Effect. *Chem. Commun.* **2013**, *49*, 8072−8074.
(32) Genin, E.; Gao, Z.; Varela, J. A.; Daniel, J.; Bsaibess, T.; Gosse, I.; Groc, L.; Cognet, L.; Blanchard-Desce, M. Hyper-Bright" Near-Infrared Emitting Fluorescent Organic Nanoparticles for Single Particle Tracking. *Adv. Mater.* **2014**, *26*, 2258−2261.
(33) Shao, A.; Xie, Y.; Zhu, S.; Guo, Z.; Zhu, S.; Guo, J.; Shi, P.; James, T. D.; Tian, H.; Zhu, W. H. Far-Red and Near-IR AIE-Active Fluorescent Organic Nanoprobes with Enhanced Tumor-Targeting Efficacy: Shape-Specific Effects. *Angew. Chem.* **2015**, *127*, 7383−7388.
(34) Lan, M.; Zhang, J.; Zhu, X.; Wang, P.; Chen, X.; Lee, C. S.; Zhang, W. Highly Stable Organic Fluorescent Nanorods for Living Cell Imaging. *Nano Res.* **2015**, *8*, 2380−2389.
(35) Zhang, J.; Liang, Y. C.; Lin, X.; Zhu, X.; Yan, L.; Li, S.; Yang, X.; Zhu, G.; Rogach, A. L.; Yu, P. K. N.; Shi, P.; Tu, L. C.; Chang, C. C.; Zhang, X.; Chen, X.; Zhang, W.; Lee, C. S. Self-Monitoring and Self-Delivery of Photosensitizer-Doped Nanoparticles for Highly Effective Combination Cancer Therapy in Vitro and in Vivo. *ACS Nano* **2015**, *9*, 9741−9756.
(36) Zhang, J.; Chen, R.; Zhu, Z.; Adachi, C.; Zhang, X.; Lee, C. S. Highly Stable Near-Infrared Fluorescent Organic Nanoparticles with a Large Stokes Shift for Noninvasive Long-Term Cellular Imaging. *ACS Appl. Mater. Interfaces* **2015**, *7*, 26266−26274.
(37) Mei, J.; Hong, Y.; Lam, J. W. Y.; Qin, A.; Tang, Y.; Tang, B. Z. Aggregation-Induced Emission: the Whole Is More Brilliant Than the Parts. *Adv. Mater.* **2014**, *26*, 5429−5479.
(38) Wu, K. C.; Ku, P. J.; Lin, C. S.; Shih, H. T.; Wu, F. I.; Huang, M. J.; Lin, J. J.; Chen, I. C.; Cheng, C. H. The Photophysical Properties of Dipyrenylbenzenes and Their Application as Exceedingly Efficient Blue Emitters for Electroluminescent Devices. *Adv. Funct. Mater.* **2008**, *18*, 67−75.
(39) Kim, H. M.; Cho, B. R. Small-Molecule Two-Photon Probes for Bioimaging Applications. *Chem. Rev.* **2015**, *115*, 5014−5055.
(40) Pond, S. J. K.; Rumi, M.; Levin, M. D.; Parker, T. C.; Beljonne, D.; Day, M. W.; Bredas, J. L.; Marder, S. R.; Perry, J. W. One- and Two-Photon Spectroscopy of Donor-Acceptor-Donor Distyrylbenzene Derivatives: Effect of Cyano Substitution and Distortion from Planarity. *J. Phys. Chem. A* **2002**, *106*, 11470−11480.
(41) Rumi, M.; Ehrlich, J. E.; Heikal, A. H.; Perry, J. W.; Barlow, S.; Hu, Z.; McCord-Maughon, D.; Parker, T. C.; Röckel, H.; Thayumanavan, S.; Marder, S. R.; Beljonne, D.; Brédas, J.-L. Structure-Property Relationships for Two-Photon Absorbing Chromophores: Bis-Donor Diphenylpolyene and Bis(styryl)benzene Derivatives. *J. Am. Chem. Soc.* **2000**, *122*, 9500−9510.
(42) Gorse, A.-D.; Pesquer, M. Intramolecular Charge Transfer Excited State Relaxation Processes in Para-Substituted N,N-Dimethylaniline: A Theoretical Study Including Solvent Effects. *J. Phys. Chem.* **1995**, *99*, 4039−4049.
(43) Uoyama, H.; Goushi, K.; Shizu, K.; Nomura, H.; Adachi, C. Highly efficient organic light-emitting diodes from delayed fluorescence. *Nature* **2012**, *492*, 234−238.
(44) Ye, J.; Chen, Z.; Fung, M. K.; Zheng, C.; Ou, X.; Zhang, X.; Yuan, Y.; Lee, C. S. Carbazole/Sulfone Hybrid D-π-A-Structured Bipolar Fluorophores for High-Efficiency Blue-Violet Electroluminescence. *Chem. Mater.* **2013**, *25*, 2630−2637.
(45) Nishimoto, T.; Yasuda, T.; Lee, S. Y.; Kondo, R.; Adachi, C. A Six-Carbazole-Decorated Cyclophosphazene as A Host with High Triplet Energy to Realize Efficient Delayed-Fluorescence OLEDs. *Mater. Horiz.* **2014**, *1*, 264−269.
(46) Blouin, N.; Michaud, A.; Leclerc, M. A Low-Bandgap Poly(2,7-Carbazole) Derivative for Use in High-Performance Solar Cells. *Adv. Mater.* **2007**, *19*, 2295−2300.
(47) Li, J.; Grimsdale, A. Carbazole-Based Polymers for Organic Photovoltaic Devices. *Chem. Soc. Rev.* **2010**, *39*, 2399−2410.
(48) Li, M.; Ni, W.; Feng, H.; Wan, X.; Liu, Y.; Zuo, Y.; Kan, B.; Zhang, Q.; Chen, Y. A Low Bandgap Carbazole Based Small Molecule for Organic Solar Cells. *Org. Electron.* **2015**, *24*, 89−95.
(49) Gracia, I.; Feringán, B.; Serrano, J. L.; Termine, R.; Golemme, A.; Omenat, A.; Barberá, J. Functional Carbazole Liquid-Crystal Block Codendrimers with Optical and Electronic Properties. *Chem. - Eur. J.* **2015**, *21*, 1359−1369.
(50) Tang, J.; Hua, J.; Wu, W.; Li, J.; Jin, Z.; Long, Y.; Tian, H. New Starburst Sensitizer with Carbazole Antennas for Efficient and Stable Dye-Sensitized Solar Cells. *Energy Environ. Sci.* **2010**, *3*, 1736−1745.
(51) Zhan, X. W.; Liu, Y. Q.; Zhu, D. B.; Liu, X. C.; Xu, G.; Ye, P. X. Large Third-Order Nonlinear Optical Response of Conjugated Copolymers Consisting of Fluorene and Carbazole Units. *Chem. Phys. Lett.* **2002**, *362*, 165−169.
(52) Tirapattur, S.; Belletête, M.; Drolet, N.; Leclerc, M.; Durocher, G. Steady-State and Time-Resolved Studies of 2,7-Carbazole-Based Conjugated Polymers in Solution and As Thin Films: Determination of Their Solid State Fluorescence Quantum Efficiencies. *Chem. Phys. Lett.* **2003**, *370*, 799−804.
(53) Lin, S. L.; Chan, L. H.; Lee, R. H.; Yen, M. Y.; Kuo, W. J.; Chen, C. T.; Jeng, R. J. Highly Efficient Carbazole-π-Dimesitylborane Bipolar Fluorophores for Nondoped Blue Organic Light-Emitting Diodes. *Adv. Mater.* **2008**, *20*, 3947−3952.
(54) Serevičius, T.; Nakagawa, T.; Kuo, M. C.; Cheng, S. H.; Wong, K. T.; Chang, C. H.; Kwong, R. C.; Xia, S.; Adachi, C. Enhanced Electroluminescence Based on Thermally Activated Delayed Fluorescence From A Carbazole-Triazine Derivative. *Phys. Chem. Chem. Phys.* **2013**, *15*, 15850−15855.
(55) Liu, X.; Sun, Y.; Zhang, Y.; Miao, F.; Wang, G.; Zhao, H.; Yu, X.; Liu, H.; Wong, W. Y. A 2,7-Carbazole-Based Dicationic Salt for Fluorescence Detection of Nucleic Acids and Two-Photon Fluorescence Imaging of RNA in Nucleoli and Cytoplasm. *Org. Biomol. Chem.* **2011**, *9*, 3615−3618.
(56) De Meulenaere, E.; Chen, W. Q.; Van Cleuvenbergen, S.; Zheng, M. L.; Psilodimitrakopoulos, S.; Paesen, R.; Taymans, J. M.; Ameloot, M.; Vanderleyden, J.; Loza-Alvarez, P.; Duan, X. M.; Clays, K. Molecular Engineering of Chromophores for Combined Second-Harmonic and Two-Photon Fluorescence in Cellular Imaging. *Chem. Sci.* **2012**, *3*, 984−995.
(57) Sun, Y.; Zhao, Y.; Liu, X.; Ren, A.; Feng, J.; Yu, X. Theoretical Investigation of The Two-Photon Absorption Properties of 3,6-Bis(4-Vinylpyridinium) Carbazole Derivatives-New Biological Fluorescent Probes. *J. Mol. Model.* **2012**, *18*, 2357−2367.
(58) Zheng, K.; Lin, W.; Tan, L.; Chen, H.; Cui, H. A Unique Carbazole-Coumarin Fused Two-Photon Platform: Development of A Robust Two-Photon Fluorescent Probe for Imaging Carbon Monoxide in Living Tissues. *Chem. Sci.* **2014**, *5*, 3439−3448.
(59) Li, J.; Bao, H.; Hou, X.; Sun, L.; Wang, X.; Gu, M. Graphene Oxide Nanoparticles as A Nonbleaching Optical Probe for Two-Photon Luminescence Imaging and Cell Therapy. *Angew. Chem., Int. Ed.* **2012**, *51*, 1830−1834.

DOI: 10.1021/acsami.6b03259
ACS Appl. Mater. Interfaces 2016, 8, 11355−11365

(60) Tang, J.; Kong, B.; Wu, H.; Xu, M.; Wang, Y.; Wang, Y.; Zhao, D.; Zheng, G. Carbon Nanodots Featuring Efficient FRET for Real-Time Monitoring of Drug Delivery and Two-Photon Imaging. *Adv. Mater.* **2013**, *25*, 6569−6574.
(61) Xu, W.; Zuo, J.; Wang, L.; Ji, L.; Chao, H. Dinuclear Ruthenium(II) Polypyridyl Complexes as Single and Two-Photon Luminescence Cellular Imaging Probes. *Chem. Commun.* **2014**, *50*, 2123−2125.
(62) Xiang, J.; Cai, X.; Lou, X.; Feng, G.; Min, X.; Luo, W.; He, B.; Goh, C. C.; Ng, L. G.; Zhou, J.; Zhao, Z.; Liu, B.; Tang, B. Z. Biocompatible Green and Red Fluorescent Organic Dots with Remarkably Large Two-Photon Action Cross Sections for Targeted Cellular Imaging and Real-Time Intravital Blood Vascular Visualization. *ACS Appl. Mater. Interfaces* **2015**, *7*, 14965−14974.
(63) Mandal, A. K.; Sreejith, S.; He, T.; Maji, S. K.; Wang, X.; Ong, S. L.; Joseph, J.; Sun, H.; Zhao, Y. Three-Photon-Excited Luminescence from Unsymmetrical Cyanostilbene Aggregates: Morphology Tuning and Targeted Bioimaging. *ACS Nano* **2015**, *9*, 4796−4805.
(64) Gao, Y.; Feng, G.; Jiang, T.; Goh, C.; Ng, L.; Liu, B.; Li, B.; Yang, L.; Hua, J.; Tian, H. Biocompatible Nanoparticles Based on Diketo-Pyrrolo-Pyrrole (DPP) with Aggregation-Induced Red/NIR Emission for In Vivo Two-Photon Fluorescence Imaging. *Adv. Funct. Mater.* **2015**, *25*, 2857−2866.
(65) Akai, N.; Kudoh, S.; Nakata, M. Lowest Excited Triplet States of 1,2- And 1,4-Dicyanobenzenes by Low-Temperature Matrix-Isolation Infrared Spectroscopy and Density-Functional-Theory Calculation. *Chem. Phys. Lett.* **2003**, *371*, 655−661.
(66) Le Questel, J.-Y.; Berthelot, M.; Laurence, C. Hydrogen-Bond Acceptor Properties of Nitriles: A Combined Crystallographic and *ab initio* Theoretical Investigation. *J. Phys. Org. Chem.* **2000**, *13*, 347−358.
(67) Porter, G.; Wilkinson, F. Primary Photochemical Processes in Aromatic Molecules. Part 5. -Flash Photolysis of Benzophenone in Solution. *Trans. Faraday Soc.* **1961**, *57*, 1686−1691.
(68) Englman, R.; Jortner, J. The Energy Gap Law for Radiationless Transitions in Large Molecules. *Mol. Phys.* **1970**, *18*, 145−164.
(69) Zhang, X.; Zhang, X.; Zou, K.; Lee, C. S.; Lee, S. T. Single-Crystal Nanoribbons, Nanotubes, and Nanowires from Intramolecular Charge-Transfer Organic Molecules. *J. Am. Chem. Soc.* **2007**, *129*, 3527−3532.
(70) Piston, D. W.; Masters, B. R.; Webb, W. W. Three-Dimensionally Resolved NAD(P)H Cellular Metabolic Redox Imaging of the In Situ Cornea with Two-Photon Excitation Laser Scanning Microscopy. *J. Microsc.* **1995**, *178*, 20−27.

DOI: 10.1021/acsami.6b03259
ACS Appl. Mater. Interfaces 2016, 8, 11355−11365